JMB

Available online at www.sciencedirect.com

SCIENCE DIRECT®

ELSEVIER

The Retinal Conformation and its Environment in Rhodopsin in Light of a New 2.2 Å Crystal Structure†

Tetsuji Okada[1,2]*, Minoru Sugihara[3], Ana-Nicoleta Bondar[4,5]
Marcus Elstner[6], Peter Entel[3] and Volker Buss[7]*

[1]*Biological Information Research Center, National Institute of Advanced Industrial Science and Technology, 2-41-6 Aomi, Koto-ku, Tokyo 135-0064 Japan*

[2]*Core Research for Evolution Science and Technology (CREST), Japan Science and Technology Corporation, Kyoto 606-8502, Japan*

[3]*Institute of Physics, University of Duisburg-Essen at Duisburg 47057 Duisburg, Germany*

[4]*Computational Molecular Biophysics, University of Heidelberg, 69120 Heidelberg Germany*

[5]*Molecular Biophysics Department, German Cancer Research Center, 69120 Heidelberg, Germany*

[6]*Institute of Physics, University of Paderborn, 33098 Paderborn Germany*

[7]*Institute of Chemistry, University of Duisburg-Essen at Duisburg, 47057 Duisburg Germany*

*Corresponding authors

A new high-resolution structure is reported for bovine rhodopsin, the visual pigment in rod photoreceptor cells. Substantial improvement of the resolution limit to 2.2 Å has been achieved by new crystallization conditions, which also reduce significantly the probability of merohedral twinning in the crystals. The new structure completely resolves the polypeptide chain and provides further details of the chromophore binding site including the configuration about the C6–C7 single bond of the 11-*cis*-retinal Schiff base. Based on both an earlier structure and the new improved model of the protein, a theoretical study of the chromophore geometry has been carried out using combined quantum mechanics/force field molecular dynamics. The consistency between the experimental and calculated chromophore structures is found to be significantly improved for the 2.2 Å model, including the angle of the negatively twisted 6-s-*cis*-bond. Importantly, the new crystal structure refinement reveals significant negative pre-twist of the C11–C12 double bond and this is also supported by the theoretical calculation although the latter converges to a smaller value. Bond alternation along the unsaturated chain is significant, but weaker in the calculated structure than the one obtained from the X-ray data. Other differences between the experimental and theoretical structures in the chromophore binding site are discussed with respect to the unique spectral properties and excited state reactivity of the chromophore.

© 2004 Elsevier Ltd. All rights reserved.

Introduction

According to the general scheme of ligand recognition by membrane proteins the binding of a diffusible agent from extracellular space triggers structural changes in the receptor leading to signal transmission and subsequent regulation of cell function. Agonist binding to G protein-coupled receptors (GPCRs), a superfamily of membrane proteins containing seven transmembrane helices, drives the receptor to assume a structure that can bind and activate the heterotrimeric G protein.[1]

Rhodopsin, the visual pigment in rod photoreceptor cells, represents a paradigm for structure–function studies of GPCRs.[2,3] Detection of the photon is mediated by the 11-*cis* isomer of retinal,

---

† This paper is dedicated to Dr Yoshimasa Kyogoku.
Abbreviations used: QM, quantum mechanics; MM, molecular mechanics; MD, molecular dynamics.
E-mail addresses of the corresponding authors:
t-okada@aist.go.jp; theobuss@uni-duisburg.de

which in the dark acts as inverse agonist on rhodopsin with an estimated half-life for thermal isomerization of 420 years.[4] In an extremely fast, highly selective and effective reaction, light triggers conversion of the 11-*cis* double bond to *trans*, which initiates the visual cascade leading to the closure of ligand-gated calcium channels and excitation of the visual nerve. Detailed analysis of the different events leading to rhodopsin activation had to await resolution of the protein at an atomic scale, the first of which appeared only a few years ago.[5]

There are currently three high-resolution structures of rhodopsin in the literature. The original 2.8 Å structure (PDB identifier 1F88)[5] was the first high-resolution structure of a GPCR and revealed all the major features of the protein that had been obtained before from experimental evidence including the results from electron cryomicroscopy.[6] A refined model (1HZX)[7] added some amino acid residues missing from the original work. A more recent structure (1L9H)[8] extended the resolution to 2.6 Å. In addition, it has located seven water molecules, two of which are close to the chromophore binding site and are probably significant for rhodopsin function.

Here, we describe and discuss the results of a new X-ray structure study of rhodopsin. The probability of merohedral twinning in the crystals has been significantly reduced due to new crystallization conditions, and as a result the resolution has been improved to 2.2 Å. In the new structural model the complete polypeptide chain has been resolved for the first time. The model provides further details of the chromophore binding site including the configuration of the C6–C7 single bond and of the photoisomerization site, from C11 to C13.

Another focus of this study is to delineate how the crystallographic model of the retinal chromophore and its environment in rhodopsin with such improved quality is consistent with theoretical considerations. Sophisticated quantum-mechanical methods are needed to adequately treat a complicated unsaturated π-electron system like the twisted retinal chromophore. Being embedded in the protein environment, the chromophore should be an ideal target for treatment by combined quantum mechanics and molecular mechanics (QM/MM). This method, proposed by Warshel more than 25 years ago,[9] is now widely applied to the study of active sites and the course of enzymatic reactions of proteins,[10] and has been used to describe the structure and dynamics of retinal-binding proteins.[11,12] We have applied a recently developed QM/MM scheme[13] which combines a self-consistent charge density functional tight binding method (SCC-DFTB)[14] with the well-established CHARMM force field.[15] Detailed examinations of the crystallographic and theoretical results demonstrate a marked advance in their consistency compared with the previous models. The possible origins and implications of some remaining differences are discussed, taking into account the recently proposed activation mechanism of rhodopsin.

Results and Discussion

X-ray crystallography at 2.2 Å resolution

We have succeeded in improving the quality of rhodopsin crystals by changing the micellar conditions for both purification and crystallization. The mixed micelle solvent composed of nonylglucoside and heptanetriol is replaced by a single detergent heptylthioglucoside. With this change, the final precipitant (ammonium sulfate) concentration required for crystallization is substantially decreased, making the manipulation of crystals much easier. The maximal X-ray diffraction spots appear up to 2.0 Å resolution, and the probability of finding crystals with the twin fraction of less than 0.2 has increased roughly from 5% to 50%. The space group ($P4_1$) is the same but the unit cell, which contains four asymmetric units composed of two rhodopsin molecules, appears to be slightly longer along the *c* axis (Table 1). The most notable difference between the current model and the previous ones is that the cytoplasmic surface region is now completed although the temperature factors of some residues are still high. We confirm that the previous trace[7,8] of the backbone around the missing part was correct. The extended helical structure of helix VI is an outstanding feature of the complete model. The third cytoplasmic loop connecting helices V and VI folds outside the rhodopsin molecule, presumably along the membrane surface (Figure 1). A part of this loop is in contact with the same part in the adjacent symmetry-related molecule in the crystal. We also added water molecules that were consistently found in the two rhodopsin

Table 1. Data collection and refinement statistics

	Data set 1	Data set 2
A. *Data collection*		
Resolution (Å)	2.45	2.2
Unit cell *a, b, c* (Å)	96.76, 96.76, 150.1	96.68, 96.68, 150.2
Twin fraction	0.02	0.18
Mosaicity (deg.)	0.56	0.46
Total observations	146,786	198,898
Unique observations	44,732	61,728
R_{merge} (%) (outer shell)[a]	10.3 (64.8)	9.3 (66.7)
Completeness (%) (outer shell)	88.2 (48.4)	88.4 (46.2)
I/σ (*I*) (outer shell)	11.3 (1.1)	11.9 (1.2)
Wilson *B* factor (Å²)	54.2	42.1
B. *Refinement*		
R_{cryst} (%)		20.0
R_{free} (%)[b]		22.2
rmsd of bonds (Å)		0.012
rmsd of angles (deg.)		1.40

Data sets 1 and 2 were collected at BL41XU of Spring-8 with an exposure time of five seconds per 1.5° oscillation for the total of 90°. The crystal-to-detector distance was 160 mm for set 1 and 140 mm for set 2. The X-ray wavelength was 1.000 Å for both the data sets.

[a] $R_{merge} = \Sigma_{hkl} \Sigma_i I_i (hkl) - <I(hkl)> | / \Sigma_{hkl} \Sigma_i I_i(hkl)$.

[b] R_{free} was calculated from a set of 5% ramdomly selected reflections that were omitted from refinement.
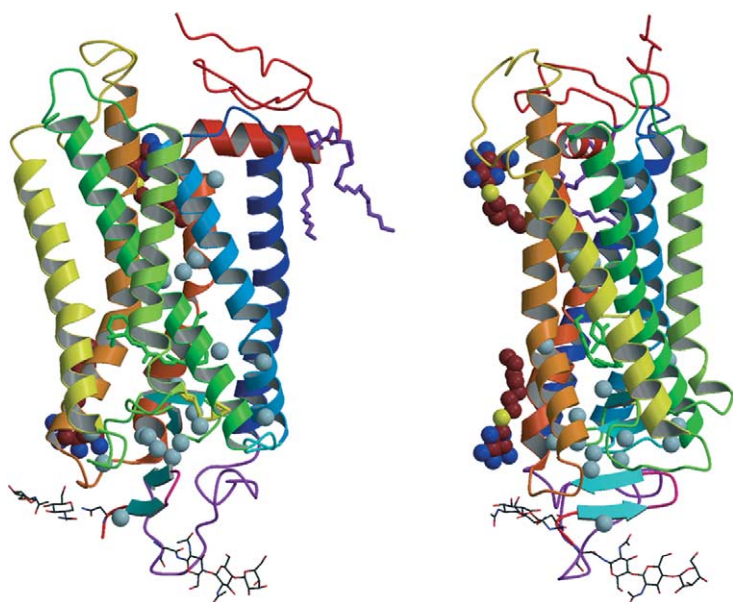
Figure 1. Crystal structure model of bovine rhodopsin at 2.2 Å. The two Figures shown are related by a 90° rotation along the vertical axis. Water molecules that are found inside the protein consistently in the two molecules of an asymmetric unit are indicated by light blue spheres. In the right Figure, two heptylthioglucoside molecules are also shown to indicate the approximate range of the transmembrane domain.

molecules in an asymmetric unit. These are mostly located in the extracellular domains, especially around the second extracellular loop connecting helices IV and V. This demonstrates that the loop interacts with the retinal chromophore while being solvated to some extent. In another point of view, the interactions of this loop with the other parts of extracellular domains would be suitable for flexible rearrangement that might occur during either photoactivation or passing of the retinal. We do not find any new water molecules that might affect the electronic state of the retinal chromophore. In the transmembrane region, the only water molecule added to the previous 2.6 Å model is in the site 1 surrounded by helices I, II, III, VI and VII[8].

Stereo images of the chromophore and its binding site are presented in Figure 2. Most importantly, the C11–C12 double bond is found to be significantly pre-twisted in the ground state. This feature strongly suggests the way isomerization occurs around this bond upon photon absorption. Another region of interest concerns the C6–C7 single bond, which defines the orientation of the β-ionone ring. In the electron density map calculated to 2.2 Å resolution, the shape of the ring becomes clearer, making the definition of the C6–C7 angle more reliable. The result supports the 6s-*cis* form with substantial negative twist. All the dihedral angles along with the bond lengths and angles are given in Tables 2–4 and are examined in more detail by comparison with the theoretical calculations later.

The arrangement of the set of residues constituting the retinal-binding pocket is almost the same as the previous crystallographic models. As shown in Figure 2, the C11–C12 double bond is in close contact with the second extracellular loop at one side while the other side has no interactions with the protein moiety. The C20 methyl group attached to C13 appears to contribute to the twist around C11–C12 through interaction with Trp265. The

orientation of the β-ionone ring is restricted by a set of hydrophobic residues in the cytoplasmic side, such as Phe212, Phe261 and Trp265.

It should be noted that the hydrogen bonded network around the chromophore mediated by two water molecules in the 2.6 Å resolution structure[8] is confirmed in the current crystallographic model. It appears to be critical for the regulation of absorption wavelength, the stabilization of protonated Schiff base and activation upon photon absorption. As shown in Figure 7, however, the theoretical calculations deviate from the crystal structure in some points, and they are examined in detail later.

Comparison with previous models

The crystallographic resolution obtained so far for rhodopsin has been insufficient to unequivocally define the functionally important parts. In fact, large deviations between the different models were found, in addition to the structurally poorly defined loops at the cytoplasmic side of the protein, in the region close to the retinal chromophore. For example, in 1L9H, the C15 retinal atom, which is directly linked to the Schiff base nitrogen, was displaced by 1.2 Å relative to its position in 1HZX, and the shift of the C16 atom (which is one of the *gem*. dimethyl groups of the ionone ring) was even larger, 1.7 Å.[16] These conflicting data might be caused by significant differences in the dihedral angles of the chromophore.

With respect to the ionone ring, the configuration is distorted 6s-*cis*, according to the new model, with a dihedral angle of −30.3° (chain A) and −31.9° (chain B), while in 1F88 the same angle is larger than −60°.[5] Similar diverging results have been reported for the central *cis*-configurated C11–C12 bond with dihedral angles C10–C11–C12–C13 ranging from −1.7° (1F88, chain B)[5] to +7.9° (1HZX, both chains).[7] The values according to the new model
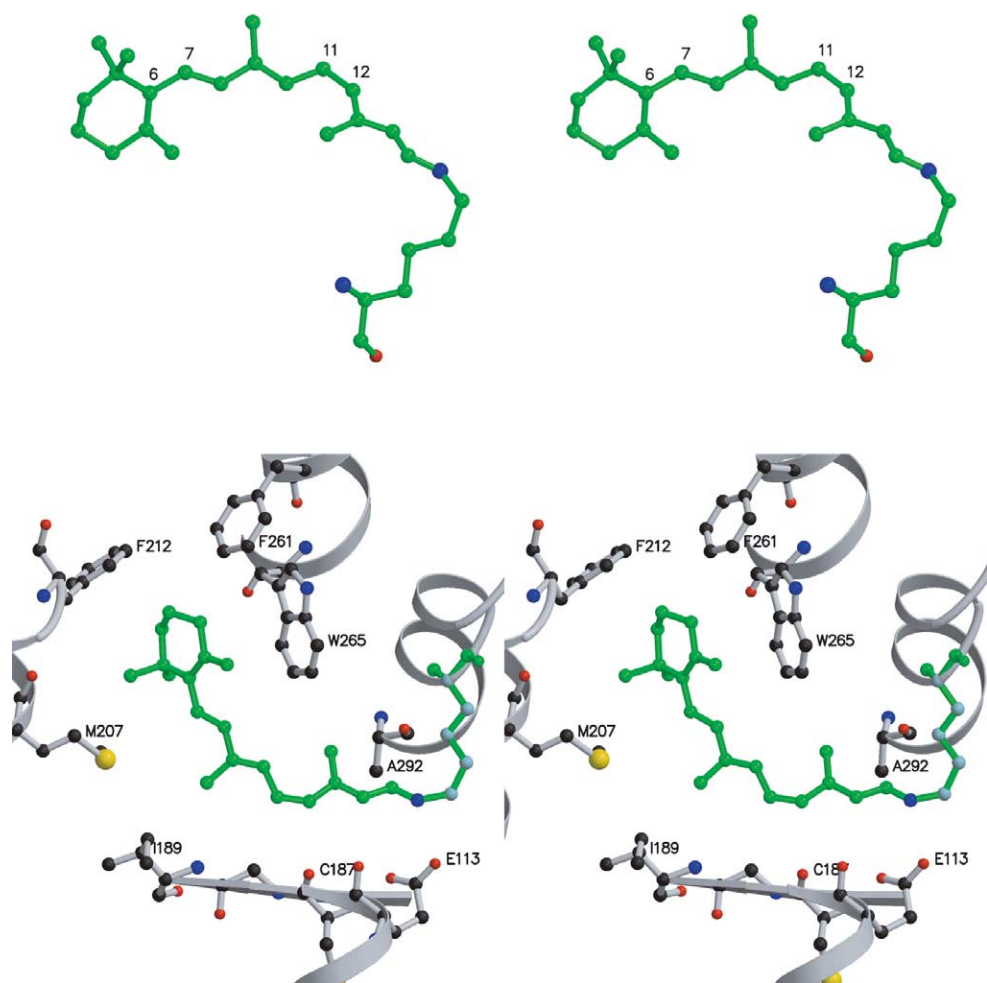
Figure 2. Retinal chromophore and its environment in the crystal. Top, stereo pair of the 11-*cis*-retinal Schiff base linked to Lys296. Nitrogen and oxygen atoms are colored in blue and red, respectively. The carbon numbers are marked only for the two bonds that are found to be significantly twisted. Bottom, stereo pair of the chromophore-binding site with some nearby amino acid residues having large contact surface with the retinal.

are −40.8° and −36.1° for chain A and chain B, respectively.

From the interaction with the protein pocket, which causes the chromophore to adopt the strained, twisted geometry, one would expect this region to be structurally rather well defined, and indeed the region around the Schiff base has the lowest crystallographic temperature factors of the protein.[17] Also, this is the region where the photoreaction is initialized and where the photonic energy has to be funnelled into an exactly predetermined way to initiate the visual cascade.

The reason for the apparent discrepancy, the accuracy of the protein backbone and the fuzziness of the chromophore conformation, might simply be due to the models employed. There exists, in the molecular mechanics part of CNS,[18] which is one of the standard pieces of refinement software for X-ray structures, a well-established set of parameters for the amino acid residues used to model protein secondary and tertiary structures. No such parameters are available for chemically unusual structures such as a twisted extended π-system, or

for a carboxylate group interacting with the delocalized charge of an extended chromophore. Thus one should not expect a region like the chromophore-binding site of rhodopsin to be modelled with the same reliability as the well-established protein backbone.

With its theoretically challenging chromophore structure in a classical protein environment, rhodopsin presents an ideal object for applying combined QM/MM. The method we use has been developed recently and is described in more detail in Materials and Methods. Linked to an efficient molecular dynamics (MD) routine that enables the system to search the conformational space accessible at ambient temperatures we have investigated the conformation of the retinal chromophore inside the protein environment against the geometries provided by the different rhodopsin models.

QM/MM modelling of the chromophore structure

Starting with models built from the X-ray data of chain A of the 2.6 Å structure[7] and chains A and B

Table 2. Experimental (plain) and calculated bond lengths (in italics, with root-mean-square deviations where applicable) of different chromophore models

	C5=C6	C6–C7	C7=C8	C8–C9
2.6 A	1.413	1.515	1.383	1.482
MD	*1.367 ± 0.019*	*1.462 ± 0.028*	*1.368 ± 0.022*	*1.444 ± 0.027*
2.2 A	1.427	1.508	1.365	1.470
MD	*1.367 ± 0.021*	*1.462 ± 0.027*	*1.368 ± 0.021*	*1.444 ± 0.025*
2.2 B	1.437	1.516	1.362	1.461
MD	*1.366 ± 0.021*	*1.464 ± 0.027*	*1.367 ± 0.021*	*1.446 ± 0.025*
pSb	*1.378*	*1.441*	*1.379*	*1.430*
pSb (COO⁻)	*1.366*	*1.458*	*1.367*	*1.443*

	C9=C10	C10–C11	C11=C12	C12–C13
2.6 A	1.352	1.486	1.371	1.480
MD	*1.392 ± 0.025*	*1.421 ± 0.026*	*1.387 ± 0.025*	*1.430 ± 0.026*
2.2 A	1.371	1.456	1.389	1.489
MD	*1.391 ± 0.022*	*1.421 ± 0.025*	*1.386 ± 0.023*	*1.431 ± 0.026*
2.2 B	1.367	1.464	1.389	1.490
MD	*1.388 ± 0.023*	*1.425 ± 0.025*	*1.383 ± 0.023*	*1.435 ± 0.025*
pSb	*1.402*	*1.406*	*1.397*	*1.414*
pSb (COO⁻)	*1.387*	*1.422*	*1.384*	*1.431*

	C13=C14	C14–C15	C15=N16	
2.6 A	1.355	1.501	1.349	
MD	*1.403 ± 0.025*	*1.415 ± 0.026*	*1.324 ± 0.023*	
2.2 A	1.353	1.428	1.326	
MD	*1.401 ± 0.023*	*1.415 ± 0.024*	*1.323 ± 0.022*	
2.2 B	1.376	1.449	1.344	
MD	*1.397 ± 0.023*	*1.421 ± 0.025*	*1.318 ± 0.022*	
pSb	*1.415*	*1.396*	*1.337*	
pSb (COO⁻)	*1.397*	*1.417*	*1.316*	

From the top, chain A of the 2.6 Å structure; corresponding MD based on this structure; chain A of the 2.2 Å structure; corresponding MD; chain B of the 2.2 Å structure; corresponding MD; optimized chromophore geometry without protein environment; optimized chromophore geometry with Glu113 only at 2.6 Å distance.

of the 2.2 Å structure, QM/MM MD simulations have been performed after simulated annealing to obtain averaged equilibrated geometries. The complete set of numerical data of the three models can be found in Tables 2–4. From these data it can be seen that all calculations converge to practically the same structure for the chromophore. This is actually not too surprising, considering how well the different models for the chromophore-binding pocket match. The largest deviations are 0.006 Å for bond lengths (the C13–C14 and C14–C15 bonds), 1.4° for bond angles (the C15N16CE angle) and 2° for dihedral angles (about the C11–C12 bond).

The graphs shown in Figures 3 to 5 and discussed in the following three sections have been organized as follows. The four graphs shown in blue continuous and broken lines and in green continuous and broken lines represent the experimental structure sets taken from chains A and B of the 2.6 Å and 2.2 Å structures, respectively. Shown in red, including error bars, are the QM/MM MD results for chain A of the 2.2 Å structure. Also included, to show how the protein-binding pocket affects the chromophore, is the chromophore geometry optimized with the same quantum-mechanical method as before, but omitting either the protein completely (orange) or including the counterion (orange broken). In the latter, the counterion was fixed in

the same position as in the simulations involving the complete pocket.

Bond lengths and bond alternation

The strong bond alternation present in the four experimental structures is obvious from the zig-zag shape displayed in the plot of consecutive bond lengths (Figure 3). Bond lengths range from 1.51 Å (the C6–C7 bond in the 2.2 Å structure) to 1.35 Å (C9–C10 bond, 2.6 Å structure). The agreement between the different experimental structures is better in the C-terminal than in the N^+-terminal region of the Schiff base. For example, the C14–C15 bond length differs by 0.7 Å, while the difference in the C6–C7 bond length is less than 0.1 Å. This might be yet another indication that the MM methods used in fitting the experimental diffraction data are better equipped to treat the part of the chromophore that is dominated by simple conjugation effects than the azomethine region where additional electronic effects due to the counterion complicate the conjugated character of the chromophore.

The calculated bond length alternation in the region from C8 to C15 is significantly weaker than found in the experiment. All single bonds are shorter than in the experiment, and the double bonds longer. Part of the reduced bond length

Table 3. Experimental and calculated bond angles (deg.) of different chromophore models

	C5C6C7	C6C7C8	C7C8C9	C8C9C10
2.6 A	117.4	119.5	132.1	117.4
MD	122.0±3.1	122.6±3.8	125.7±3.3	117.4±3.1
2.2 A	121.4	131.8	131.2	115.4
MD	121.9±2.9	122.3±3.5	125.9±3.2	117.1±2.8
2.2 B	120.8	132.3	130.5	115.1
MD	121.9±3.0	122.6±3.5	125.9±3.2	117.4±2.8
pSb	123.1	126.8	123.5	117.7
pSb (COO⁻)	122.7	124.9	124.8	117.3

	C9C10C11	C10C11C12	C11C12C13	C12C13C14
2.6 A	124.9	129.2	138.5	114.2
MD	124.1±3.3	127.8±3.2	129.8±3.2	117.3±3.0
2.2 A	125.7	122.3	131.7	112.9
MD	124.2±3.1	127.7±3.2	129.8±3.2	117.1±2.9
2.2 B	126.0	122.9	131.5	112.7
MD	123.9±3.0	127.9±3.2	129.6±3.1	117.1±2.8
pSb	124.7	129.4	130.9	116.5
pSb (COO⁻)	125.9	128.7	130.6	117.4

	C13C14C15	C14C15N16	C15N16CE	C12C13C20
2.6 A	125.0	117.9	134.4	121.4
MD	124.5±3.4	120.9±3.0	122.3±3.7	121.7±3.4
2.2 A	127.4	118.3	135.2	123.4
MD	124.5±3.1	121.0±3.0	121.7±3.5	121.7±3.2
2.2 B	128.4	119.2	134.5	122.9
MD	124.5±3.1	121.0±3.0	120.9±3.5	121.6±3.1
pSb	125.8	121.4	123.9	122.4
pSb (COO⁻)	124.0	120.8	123.6	121.6

Table 4. Experimental and calculated dihedral angles (deg.) of different chromophore models

	C6–C7	C7=C8	C8–C9	C9=C10
2.6 A	−77.4	−172.9	−149.3	179.8
MD	−43.0±9.4	−178.3±7.4	173.0±9.9	171.5±7.9
2.2 A	−30.3	−174.8	171.5	−176.0
MD	−42.6±9.0	−177.0±7.4	172.7±9.2	173.0±7.4
2.2 B	−31.9	−176.8	167.0	−176.4
MD	−43.4±9.3	−178.4±7.0	172.8±9.7	173.0±7.2
pSb	−28.2	−178.9	174.6	179.1
pSb (COO²⁻)	−34.3	−177.7	175.9	−179.7

	C10–C11	C11=C12	C12–C13	C13=C14
2.6 A	162.5	0.0	171.5	172.1
MD	174.3±9.1	−18.6±9.1	170.2±8.1	173.4±7.9
2.2 A	173.2	−40.8	−173.5	170.9
MD	174.1±8.8	−17.7±9.1	169.5±8.1	174.2±7.2
2.2 B	173.9	−36.1	178.6	171.2
MD	173.2±9.0	−16.6±8.9	169.0±8.2	174.5±7.1
pSb	178.9	−3.1	179.2	179.9
pSb (COO⁻)	179.2	−1.6	179.4	−177.4

	C14–C15	C15=N16	C11C12C13C20
2.6 A	135.5	−178.9	−9.1
MD	179.5±8.7	170.4±7.2	−13.9±9.5
2.2 A	164.6	−167.9	5.2
MD	179.0±8.3	170.3±6.8	−14.0±9.7
2.2 B	178.6	−166.0	−3.0
MD	178.5±8.5	170.2±7.6	−14.5±9.8
pSb	179.7	180.0	−1.3
pSb (COO⁻)	−176.9	−176.8	−1.8

See Table 2 for details.
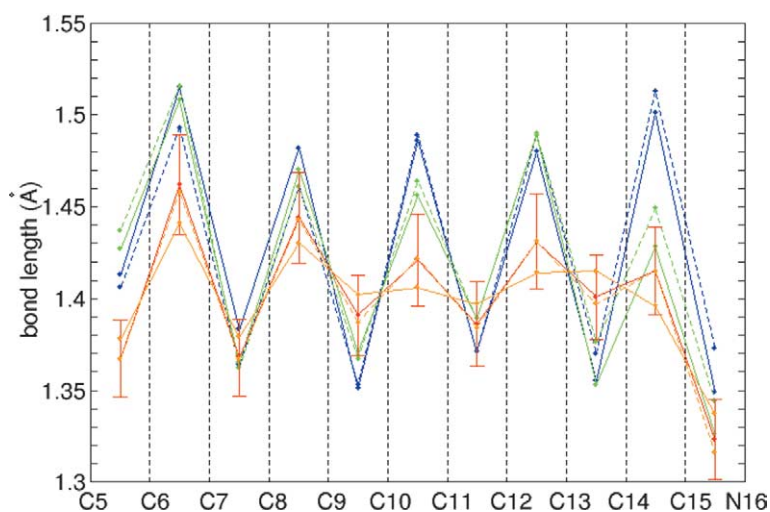
Figure 3. Bond lengths along the conjugated carbon chain. The experimental structure sets taken from chains A and B of the 2.6 Å and 2.2 Å structures are shown as blue continuous and broken lines and in green continuous and broken lines, respectively. Shown in red, including error bars, are the QM/MM MD results for chain A of the 2.2 Å structure. The free chromophore geometry optimized with the SCC-DFTB method is shown in orange (protein omitted completely) and in orange broken (including the counterion only). This color code is used also in Figures 4 and 5.
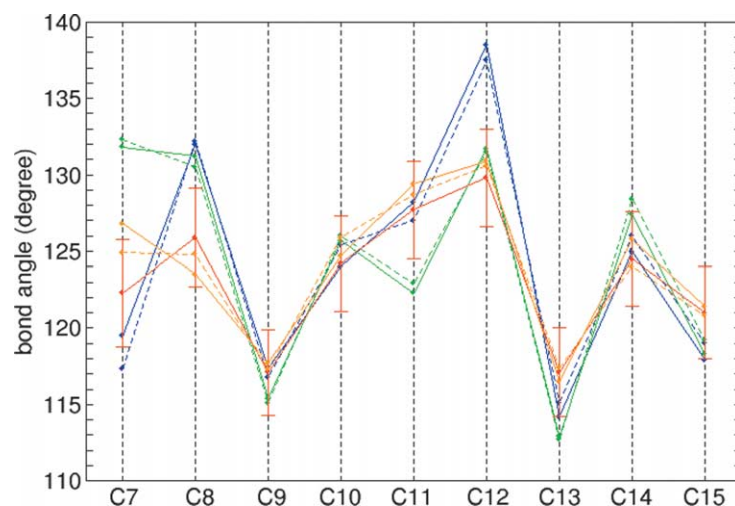
Figure 4. Bond angles along the conjugated carbon chain.
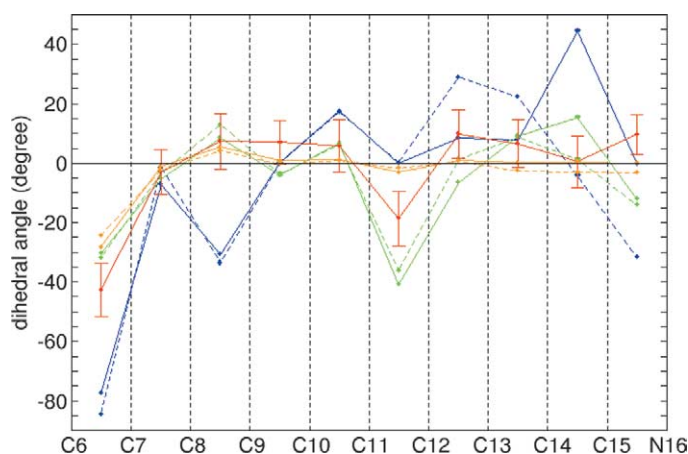
Figure 5. Dihedral angles along the conjugated carbon chain showing the deviations from either the *cis* (0°) or the *trans* (180°) configuration.

alternation is a consequence of the quantum-mechanical method on which the calculations are based. π-Electron conjugation profits strongly from correlation energy, which is partly included in density function theory (DFT) on which the SCC-DFTB-method is based. As a consequence DFT calculations are biased towards delocalization of conjugated double bonds and tend to reduce bond

alternation relative to Hartree–Fock (HF) methodology, which puts more emphasis on the description of electrons as pairs. We have found[19] that HF-calculated bond lengths agree very well with the crystal structure reported for *N*-methyl-*N*-phenyl-retinal iminium perchlorate;[20] the agreement with two retinylidene iminium salts[21] is not quite as good. Because of the speed of DFT-based quantum-mechanical optimization procedures compared to HF most QM/MM schemes rely on the former for the quantum part; however, it is advisable to keep in mind that the calculated bond alternation may be actually too low.

How the bond alternation changes as a function of the environment can be seen by comparing the three calculated structures of the chromophore depicted in the same Figure. The free protonated Schiff base displays already significant bond alternation, especially in the C-terminal region far away from the positive nitrogen atom. Placing the counterion into the model opposite the nitrogen atom localizes the positive charge of the chromophore and changes its character from a cyanine to a polyene type by reducing the relative weight of charge-resonating structures.[22] This amplifies, as expected, bond alternation throughout the chromophore. The resulting structure is virtually identical with the one obtained from the MD simulation including the whole protein. We conclude that bond alternation is determined almost completely by the presence of the counterion and is not a sensible function of the remaining protein environment. This is important in view of the fact that the counterion severely affects the UV/visible spectral properties of the chromophore.[23]

Recently the carbon–carbon bond lengths of the bovine rhodopsin chromophore were determined by double-quantum solid-state NMR.[24] The C14–C15 bond (1.428 Å) was found to be longer than the C12–C13 bond (1.410 Å). This agrees with the 2.6 Å crystal structure;[8] however, in the new 2.2 Å structure these two bond lengths are reversed, in agreement with the quantum-mechanical structure calculations. The MD simulations converge to practically identical values, the C14–C15 bond to 1.415 Å and the C12–C13 bond to 1.431 Å, in good agreement with the published crystal structures.[20,21]

Bond angles

Experimental and calculated bond angles along the conjugated chain are shown in Figure 4. Both reveal a distinctly alternating pattern: bond angles centered at odd-numbered carbon atoms are always smaller than their direct neighbors. This anomaly has been observed both experimentally[25] and from computational studies[26] of cyanine-type dyes and can be correlated with hybridization changes due to alternating atomic charges.[27] Superposed on this regular alternation pattern of the bond angles are the effects due to the peculiarities of the chromophore: the small values at C9 and C13 result from the spacious methyl substituents at these positions,

and the angles at C11 and C12 are widened to ease the strain of the 11-*cis*-configured double bond.

The agreement between calculated and experimentally determined bond angle is generally very good; the large discrepancies observed for the C6–C7–C8 bond angle reflects the highly divergent orientation of the β-ionone ring in the different models. As expected, steric strain is expressed in different bond angles and dihedral angles rather than bond lengths.

Dihedral angles

Dihedral angles determine the conformation of the chromophore more than bond lengths and bond angles. Also, dihedral angles react more sensitively to changes in the environment because of the small force constants involved. This can be seen very clearly in the calculated chromophore conformations shown in Figure 5, which show the deviations from either the *cis* (0°) or the *trans* (180°) configuration. In the absence of the forces exerted by the protein pocket the chromophore is essentially planar. Except for the C8–C9 bond the dihedral angles deviate at most by 5° from the zero line, which corresponds to the perfectly planar chromophore with 0 and 180° dihedral angles only. The red line shows the effect of the protein and how it induces non-planar twists into the carbon chain: all dihedrals from C8 to C14 are twisted from planarity by positive values of about 10°; the only dihedral angle that comes out negative (−18°) is the C11–C12 *cis* configured double bond. Note also the strong negative twist of the C6–C7 bond, which indicates the orientation of the β-ionone ring relative to the polyene chain.

It should again be pointed out that this chromophore conformation is obtained regardless of the starting geometry. The structure is essentially identical with the one published recently[28] where the chromophore was optimized inside the protein pocket of the 2.8 Å resolution structure. The only deviations are observed in somewhat smaller twists of the C6–C7 (−35° *versus* −43°) and the C11–C12 bond (−11° *versus* −18°), possibly on account of the rigidity of the protein pocket.

Comparison of the MD structure with the experiment reveals major differences with the 2.6 Å structure (especially the C6–C7 and C8–C9 twist; the region from C10 to N16), while the agreement with the 2.2 Å structure is significantly better. Major differences remaining are the C6–C7 angle (experimental −30°, calculated −43°), and the C14–C15 angle (15° *versus* 0°). The agreement in the central part of the chromophore is better than Figure 5 seems to suggest, since the dihedrals are all interrelated, leading to a certain overall twist of the chromophore. In the 2.6 Å structure the twist is localized on the C10–C11 and the C11 to C14 bonds, with the 11-*cis*-bond remaining planar. In the 2.2 Å structure the twist is concentrated on the C11–C12 bond, and the adjacent bonds are less distorted. The calculated structure appears to represent a

compromise, with the twist necessary to fit the chromophore into the binding pocket evenly distributed between the four neighboring bonds. Electronically this makes sense because distributing the distortion over several bonds causes less disruption in conjugation.

The sign of the C6–C7 dihedral angle has been shown by experimental CD studies on enantiomeric 6s-*cis*-locked retinal derivatives to be negative,[29] in agreement with all published rhodopsin structures[5,7,8] and theoretical predictions.[30] There is as yet no indication that the orientation of the β-ionone ring, including the absolute conformation, i.e. the sign of the dihedral angle, is a determining factor in the reactivity of the chromophore. The situation is decidedly different in the middle of the chromophore, where the primary step of the visual process, photo-isomerization of the 11–12 double bond from *cis* to *trans*, takes place. Anticipating the ensuing rotation of the chromophore torsion along this bond might actually be a pre-requisite for this exceedingly stereoselective and efficient reaction.[31] An indication of this torsion is the inherent chirality of the chromophore, which is manifest in the chiroptical properties of the pigment in the visible region.[32–34] For a quantitative estimate of the overall twist of the conjugated chain, use was made of solid-state NMR spectroscopy of isotopically labelled retinal derivatives,[35,36] from which an angle of ∼42° between the two planes approximated by the C7–C10 and the C13–C15 fragments was deduced. The corresponding values in the experimental models are ∼46° (chain A) and ∼63° (chain B) in the 2.2 Å structure, and ∼10° (chain A) in the 2.6 Å structure. In the calculated structure this angle is ∼36°, in satisfactory agreement with experiment.

With respect to the absolute sense of twist of the chromophore, agreement has been reached lately based on theoretical considerations[37] and experimental studies[38] that the twist is negative about the C11–C12 and positive about the C12–C13 bond. The MD simulations agree with these analyses, giving values of $-18(\pm 9)°$ and $+170(\pm 9)°$, respectively,

for the two dihedrals. Figure 6, which shows the time-dependent change of three key dihedral angles during the equilibrium MD runs, gives an impression of how the seemingly high margins of error come about. The C12–C13 dihedral angle can reach extreme values between 140 and 195° at the simulated temperature of 300 K. Despite these large thermal fluctuations of the dihedral angles the structure is completely stable. Neither a switch of the C11–C12 nor of the C6–C7 bond into the oppositely twisted form has ever been observed during the simulation process.

The question which of the two possible twisted conformations of the chromophore are realized in the protein pocket is only partly academic. The agreement of the calculations with the experiment is a strong indication for the correct modelling of the binding pocket. However, even more important, the twist of the C11–C12 double bond determines the sense of rotation of the chromophore following photoexcitation. Only the clockwise movement of the C12–C13 fragment against the C11–C10 bonds is supported by the out-of-plane twist of the C13 methyl, with logical consequences for the absolute conformation of the twisted bathorhodopsin intermediate.

The hydrogen bonded network at the chromophore-binding site

The position of the Glu113 counterion opposite the Schiff base binding site of the chromophore has not changed much since the first published rhodopsin structure:[5] the carboxylate group is oriented approximately coplanar with the C15–N16–Cε fragment of the Schiff base, with one of the oxygen atoms within hydrogen-bonding distance (3.3 Å) of the Schiff base nitrogen atom. In the later models, slightly different values have been reported (3.13 Å in chain A 1L9H, 3.45 Å and 3.28 Å in the present study). In the calculations, all these values converge to a value, 2.60(±0.09) Å, which is significantly shorter than the experimental data. The evidence, experimental and theoretical, agrees
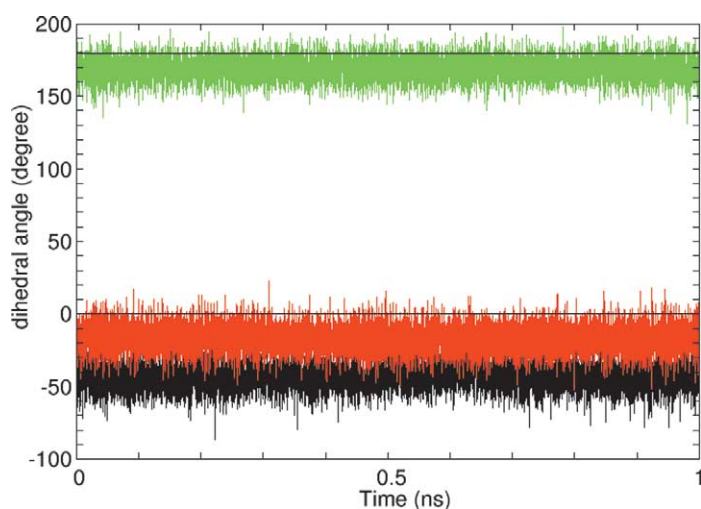
Figure 6. Time-course of a typical MD run. Three selected dihedral angles as a function of time: C6–C7 (in black), C11–C12 (in red), C12–C13 (in green).
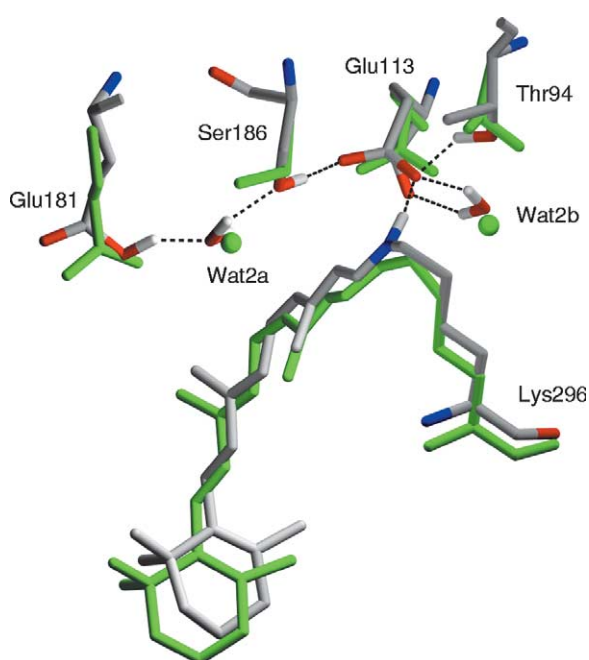
Figure 7. The hydrogen bonded network from Thr94 to Glu181 after MD equilibration. The corresponding crystal structure (chain A, 2.2 Å) is shown in green. Dotted lines indicate the hydrogen bonds observed after simulations. The hydrogen bonds from Glu113 to Thr94 and Ser186 are not evidenced by the crystal structure.

that the distance is too small to allow for a water molecule to bridge the hydrogen bond. However, a more accurate determination of this crucial bond distance is needed because the position of the counterion strongly influences the absorbance of the chromophore.

In a recent paper,[39,40] we have analyzed in detail the different factors contributing to the extraordinary stability of the protonated Schiff base in the presence of the strongly basic carboxylate counterion. Based on the results of both HF and DFT it was found that the determining factor, which keeps the proton at the Schiff base nitrogen atom rather than the carboxylate oxygen atom, is the very short distance between the two centers and the concomitant gain in electrostatic energy. Increasing the distance from 2.60 Å to 3.20 Å costs 10.9 kcal/mol in energy, which would be enough to effectively deprotonate the Schiff base.

The water molecule Wat2b, which is found near Glu113,[8] is part of the complex counterion that stabilizes the protonated state of the chromophore. Rotating the polar side-chains of Thr94 and Ser186 into a suitable orientation, a hydrogen bonding network is formed which is stable during all MD simulations including the extended 1 ns runs. In this network the Thr94 hydroxyl group binds to the Glu113 carboxylate oxygen atom, which is involved in the salt-bridge with the chromophore. This oxygen atom also coordinates with Wat2b, which

forms a bridge to the Glu113 backbone. The second oxygen atom of the carboxylate group is connected to the Ser186 hydroxyl group and the peptide backbone hydrogen atom of Cys187. Wat2a is involved in three hydrogen bonds to Ser186, to the backbone oxygen atom of Cys187, and to the OH group of Glu181. From Glu181 the network extends further to Tyr268 and Tyr192. This extended network, which is shown in Figure 6, has also been postulated on the basis of MM MD simulations.[41]

The network may form the basis for the counterion switch from Glu113 to Glu181 during formation of the meta I state of rhodopsin.[42–44] In the dark state it stabilizes the peculiar charge distribution of the chromophore at the binding site. Our calculations[39,40] have shown that a major contributing factor for keeping the Schiff base nitrogen atom protonated is the involvement of Glu113 in hydrogen bonding, which reduces its basicity. The strongest of these bonds is the one to Thr94, but bonding to Wat2b stabilizes the negatively charged counterion even further.

These results from simulation studies would explain the stabilization mechanism for the protonated state of the retinal Schiff base and are also consistent with the counterion switch hypothesis for the activation process in rhodopsin. It must be pointed out, however, that the crystal structure models at 2.6 Å and 2.2 Å resolutions differ in some connectivity of the network from the theoretical results and the model proposed in the counterion switch mechanism. There is no crystallographic evidence for direct coordination of Thr94 and Ser186 to Glu113. One consequence of this might be the longer distance of Glu113 to the Schiff base nitrogen atom. Taking the crystallographic position of the C$^\alpha$ atom of Glu113 into account, neither of the two side-chain oxygen atoms is likely to reach within 3 Å from the nitrogen atom. Therefore, a possible problem in crystallography, such as radiation damage, does not appear to explain the inconsistency with the theoretical result. Further crystallographic and theoretical studies on the photoreaction intermediates of rhodopsin would be needed to reconcile these issues.

Conclusion

A new crystal structure of bovine rhodopsin at 2.2 Å resolution has been presented as well as a new simulated model for the ground state conformation of the chromophore based on this and several other recent geometries. The 2.2 Å structure completes the description of the protein backbone and is in general agreement with earlier diffraction studies. The structures of 11-*cis*-retinal chromophore and its binding site have been defined with greater precision than ever before, demonstrating a significant pre-twist of C11–C12 double bond, which is critical for the function of rhodopsin. The hydrogen bonded network mediated by two water molecules around the chromophore is confirmed to be the

same as that proposed with 2.6 Å data. We have also examined the quantum-mechanical region of the protein, i.e. the chromophore including the counterion complex, by applying embedded quantum-chemistry. Independent of the starting geometry taken from the present or from earlier experimental simulations, data converge to practically the same structure, which shows slight, but distinct differences from all experimental structures published so far. Bond length alternation is weaker and the distance between the chromophore and the counterion is smaller than determined in the diffraction structures. Both are determining factors for the excited state properties of the chromophore and need further studies. With respect to the deformation imposed on the chromophore by the protein, the results are in complete agreement with earlier structures and should present viable starting points for modelling the geometries of the photoreaction intermediates.

Materials and Methods

Preparation and crystallization of bovine rhodopsin

Three-dimensional crystals of bovine rhodopsin were grown by hanging-drop, vapor-diffusion at 10 °C with conditions modified from previous studies.[8] Rhodopsin (6–8 mg/ml) purified in heptylthioglucoside micelles was mixed with a crystallization solution containing 6–12 mM β-mercaptoethanol, 0.1–0.5% heptylthioglucoside and 0.5–0.7 M ammonium sulfate. Some of the crystals were grown in the presence of a low concentration (0.01–0.05%) of Na/K silicate–acetate mixture that was found to be effective in stabilizing the sample. An aliquot of 4–10 μl of the mixed sample was dispensed on a siliconized coverslip, which was then fixed with paraffin oil on a well of a culture plate. The reservoir solution for vapor diffusion contained 20–30 mM Mes (pH 5.9–6.1) and various concentrations of ammonium sulfate (2.5–3.0 M). The course of crystallization was examined with a microscope using dim red light (>650 nm) to prevent the photoreaction of samples. Cryoprotectant solution containing 15% (w/v) trehalose was added to the hanging drop and crystals were flash-frozen in liquid nitrogen.

X-ray data collection and structure determination

All of the X-ray diffraction data sets were collected on a MAR165 CCD detector at BL41XU of SPring-8, Harima, Japan, with the beam wavelength of 1 Å. The temperature of the nitrogen gas at the position of the crystal was kept at 90 K during data collection.

For structure refinement the previously determined model at 2.6 Å resolution was used as starting geometry. First we used the data set 1 in Table 1, which contained quite a little fraction of twinning. After rigid body refinement, both $2F_o - F_c$ and $F_o - F_c$ maps were used in Xfit[45] to build the residues in the third cytoplasmic loop and C-terminal tail that were missing so far. The complete model of bovine rhodopsin for the two molecules in an asymmetric unit was then subjected to simulated annealing, energy minimization and *B*-factor refinement of CNS.[18] The bond and bond angle parameters for retinal were initially taken from the averages of 14 atomic coordinates deposited for archaebacterial retinal proteins

with resolution higher than 2.5 Å and then allowed to change under medium restraints during refinement. For the dihedral angles of retinal, a set of uniform and weak restraints was found to be appropriate for obtaining the best fit to experimental electron density. The present crystallographic refinement is different from all previous ones in that no biased constraints, especially at the C11–C12 bond, were applied for the dihedral angles of retinal. The crystallographic data at the final cycles of refinement using data set 2 are listed in Table 1.

Model building for simulation

The initial geometries were taken from the X-ray structures with 2.2 Å and 2.6 Å resolutions except for the orientation of two amino acid residues (see below). The 2.2 Å model contains the complete amino sequence, and both chain A and chain B were used. Of the 2.6 Å model, chain A was chosen because it is a better-refined model with fewer residues missing. These missing residues, 236–240 and 331–333, were inserted into the model manually. Palmitoyl groups, carbohydrate moieties and lipids are not included in the model.

All metal ions (Zn^{2+} and Hg^{2+}) were replaced by water molecules. The models contain 21 (2.2 Å resolution) or 15 (2.6 Å resolution) water molecules, two of which appear near the chromophore (Wat2a and Wat2b). Glu122 and Glu181 were assumed to be neutral[46,47] and as a consequence the retinal-binding pocket is charge neutral as predicted by two-photon spectroscopy.[48] All histidine residues were assumed to be protonated, His100, 195, 211, and 278 at N^δ, His65 and 152 at N^ϵ. Except for Asp83, which is neutral,[46] all other titratable groups were assumed to be charged. A disulfide bond is present between Cys110 and 187. Previous calculations[39,40] have shown that the Thr94 hydroxyl group forms a hydrogen bond with Glu113 stabilizing the protonated state of the retinal Schiff base. Also, recently an extended hydrogen bonded network extending from Glu131 to Glu181 *via* Ser186 and Wat2a has been postulated.[42] In order to accommodate this evidence we rotated the side-chains of Ser186 and Thr94 about the C^α–C^β bonds into the proper positions for hydrogen bond formation with the carboxylate oxygen atoms of Glu131.

Molecular dynamics simulation

The quantum-mechanical part of the system included the chromophore, Lys296, Glu113, Thr94 and Wat2b (85 atoms in all, including the linking hydrogen atoms). For the treatment of the QM part we employed the SCC-DFTB method, while the surrounding protein was treated by the CHARMM force field with parameter set 22.[13] A total of 111 amino acid residues next to the chromophore were considered mobile, and the remaining environment was subjected to harmonic constraints in order to preserve the overall shape of the protein.

MD simulations were performed for the three models described above to determine the equilibrium conformation of the chromophore in rhodopsin. The models built from the X-ray structures were first minimized and heated to 300 K using a MD run of 20 ps. For each model, ten sample MD runs were followed for 200 ps MD at 300 K using the Nosé canonical ensemble and two of the MD runs were continued to 1 ns to confirm that the structures had equilibrated properly.

Generation of Figures

were drawn with programs MOLSCRIPT[49] and Raster3D.[50]

Atomic coordinates

The coordinates of the 2.2 Å resolution structure of rhodopsin have been deposited in the RCSB Protein Data Bank. The accession code is 1U19.

Acknowledgements

References

1. Bockaert, J., Claeysen, S., Bécamel, C., Pinloche, S. & Dumuis, A. (2002). G protein-coupled receptors: dominant, players in cell–cell communication. *Int. Rev. Cytol.* **212**, 63–132.

2. Hubbell, W. L., Altenbach, C., Hubbell, C. M. & Khorana, H. G. (2003). Rhodopsin structure, dynamics, and activation: a perspective from crystallography, site-directed spin labeling, sulfhydryl reactivity,and disulfide cross-linking. *Advan. Protein Chem.* **63**, 243–290.

3. Baldwin, J. M., Schertler, G. F. X. & Unger, V. M. (1997). An alpha-carbon template for the transmembrane helices in the rhodopsin family of G-protein-coupled receptors. *J. Mol. Biol.* **272**, 144–164.

4. Schnapf, J. L. & Baylor, D. (1987). How photoreceptor cells respond to light. *Sci. Am.* **256**, 32–39.

5. Palczewski, K., Kumasaka, T., Hori, T., Behnke, C. A., Motoshima, H., Fox, B. A. *et al.* (2000). Crystal structure of rhodopsin: a G protein-coupled receptor. *Science*, **289**, 739–745.

6. Schertler, G. F. X. & Hargrave, P. A. (2000). Preparation and analysis of two-dimensional crystals of rhodopsin. *Methods Enzymol.* **315**, 91–107.

7. Teller, D. C., Okada, T., Behnke, C. A., Palczewki, K. & Stenkamp, R. E. (2001). Advances in determination of a high-resolution three-dimensional structure of rhodopsin, a model of G-protein-coupled receptors (GPCRs). *Biochemistry*, **40**, 7761–7777.

8. Okada, T., Fujiyoshi, Y., Silow, M., Navarro, J., Landau, E. M. & Shichida, Y. (2002). Functional role of internal water molecules in rhodopsin revealed by X-ray crystallography. *Proc. Natl Acad. Sci. USA*, **99**, 5982–5987.

9. Warshel, A. & Levitt, M. (1976). Theoretical studies of enzymatic reactions: dielectric, electrostatic and steric stabilization of the carbonium ion in the reaction of lysozyme. *J. Mol. Biol.* **103**, 227–249.

10. Monard, G. & Merz, K. M. (1999). Combined quantum mechanical/molecular mechanical methodologies applied to biomolecular systems. *Accts Chem. Res.* **32**, 904–911.

11. Hayashi, S. & Ohmine, I. (2000). Proton transfer in bacteriorhodopsin: structure, excitations, IR spectra, and potential energy surface analyses by an *ab initio* QM/MM method. *J. Phys. Chem. B*, **104**, 10678–10691.

12. Warshel, A. & Chu, Z. T. (2001). The nature of the surface crossing process in bacteriorhodopsin: computer simulations of the quantum dynamics of the primary photochemical event. *J. Phys. Chem. B*, **105**, 9857–9871.

13. Cui, Q., Elstner, M., Kaxiras, E., Frauenheim, T. & Karplus, M. (2001). A QM/MM implementation of the self-consistent charge density functional tight binding (SCC-DFTB) method. *J. Phys. Chem. B*, **105**, 569–585.

14. Elstner, M., Porezag, D., Jungnickel, G., Elsner, J., Haugk, M., Frauenheim, T. *et al.* (1998). Self-consistent-charge density-functional tight-binding method for simulations of complex materials properties. *Phys. Rev. B*, **58**, 7260–7268.

15. Mackerell, A., Bashford, D., Bellott, M., Dunbrack, R., Evanseck, J. Field, M. *et al.* (1998). All-atom empirical potential for molecular modeling and dynamics studies of proteins. *J. Phys. Chem. B*, **102**, 3586–3616.

16. Mirzadegan, T., Benkö, G., Filipek, S. & Palczewski, K. (2003). Sequence analysis of G-protein coupled receptors: similarities to rhodopsin. *Biochemistry*, **42**, 2759–2767.

17. Okada, T., Ernst, O. P., Palczewski, K. & Hofmann, K. P. (2001). Activation of rhodopsin: new insights from structural and biochemical studies. *Trends Biochem. Sci.* **26**, 318–324.

18. Brünger, A. T., Adams, P. D., Clore, G. M., DeLano, W. L., Gros, P. Grosse-Kunstleve, R. W. *et al*. (1998). Crystallography & NMR system: a new software suite for macromolecular structure determination. *Acta Crystallog. sect. D*, **54**, 905–921.

19. Terstegen, F. & Buss, V. (1998). Influence of DFT calculated electron correlation on energies and geometries of retinals and of retinals derivatives related to the bacteriorhodopsin and rhodopsin chromophores. *J. Mol. Struct. (Theochem)*, **430**, 209–218.

20. Santarsiero, B. D. & James, M. N. (1990). Crystal structure of *N*-methyl-*N*-phenylretinal iminium perchloreate: a structural model for the bacteriorhodopsin chromophore. *J. Am. Chem. Soc.* **112**, 9416–9418.

21. Elia, G. R., Childs, R. F., Britten, J. F., Yang, D. S. C. & Santarsiero, B. D. (1996). Structure and wavelength modification in retinylidene iminium salts. *Can. J. Chem.* **74**, 591–601.

22. Schreiber, M., Buss, V. & Sugihara, M. (2003). Exploring the opsin shift with *ab initio* method: geometry and counterion effects on the electronic spectrum of retinal. *J. Chem. Phys.* **119**, 12045–12048.

23. Hu, J., Griffin, R. G. & Herzfeld, J. (1994). Synergy in the spectral tuning of retinal pigments:complete accounting for the opsin shift in bacteriorhodopsin. *Proc. Natl Acad. Sci. USA*, **91**, 8880–8884.

24. Carravetta, M., Zhao, X., Johannessen, O. G., Lai, W. C., Verhoeven, M. A. Bovee-Geurts, P. H. M. *et al*. (2004). Protein-induced bonding perturbation of the rhodopsin chromophore detected by double-quantum solid-state NMR. *J. Am. Chem. Soc.* **126**, 3948–3953.

25. Dähne, L., Grahn, W., Jones, P. G. & Chrapkowski, A.

(1994). The "tube" structure of 1,7-(dimethylamino)-heptamethinium tetrafluoroborate, a streptocyanine dye. *Z. Kristallog.* **209**, 514–516.

26. Buss, V., Schreiber, M. & Fülscher, M. P. (2001). Nonempirical calculation of polymethine excited states. *Angew. Chem. Int. Ed.* **40**, 3189–3190.

27. Kulpe, S., Zedler, A., Dähne, S. & Nolte, K. D. (1973). Experimental evidence of bond-angle and hybridisation alternation caused by π-electron density alternation. *J. Prakt. Chem.* **315**, 865–872.

28. Sugihara, M., Buss, V., Entel, P., Elstner, M. & Frauenheim, T. (2002). 11-*cis*-Retinal protonated schiff base: influence of the protein environment on the geometry of the rhodopsin chromophore. *Biochemistry,* **41**, 15259–15266.

29. Fujimoto, Y., Ishihara, J., Maki, S., Fujioka, N., Wang, T. Furuta, T. *et al.* (2001). On the bioactive conformation of the rhodopsin chromophore: absolute sense of twist around the 6-*s-cis* bond. *Chem. Eur. J.* **7**, 4198–4204.

30. Buss, V. (2001). Inherent chirality of the retinal chromophore in rhodopsin—a nonempirical theoretical analysis of chiroptical data. *Chirality,* **13**, 13–23.

31. Buss, V., Weingart, O. & Sugihara, M. (2000). Fast photoisomerization of a rhodopsin model—an *ab initio* molecular dynamics study. *Angew. Chem. Int. Ed.* **39**, 2784–2786.

32. Crescitelli, F., Mommaerts, W. F. H. & Shaw, T. I. (1966). Circular dichroism of visual pigemnts in the visible and ultraviolet spectral regions. *Proc. Natl Acad. Sci. USA,* **56**, 1729–1734.

33. Ito, M., Kodama, A., Tsukida, Y., Fukada, Y., Shichida, Y. & Yoshizawa, T. (1982). A novel rhodopsin analogue possesing the cyclopentatrienylidene structure as the 11-*cis*-locked and the full planar chromophore. *Chem. Pharm. Bull.* **30**, 1913–1916.

34. Wada, A., Sakai, M., Imamoto, Y., Shichida, Y., Yamauchi, M. & Ito, M. (1997). Synthesis of (11Z)-8,18-ethanoretinal and a conformational study of the rhodopsin chromophore. *J. Chem. Soc. Perkin Trans. 1,* **12**, 1773–1777.

35. Mathies, R. A. & Lugtenburg, J. (2000). The primary photoreaction of rhodopsin. In *Handbook of Biological Physics* (Stavenga, D. G., De Gripp, W. J. & Pugh E. N., Jr.), vol. 3, p. 55, Elsevier, Amsterdam.

36. Verdegem, P. J. E., Bovee-Geurts, P. H. M., de Grip, W. J., Lugtenburg, J. & de Groot, H. J. M. (1999). Retinylidene ligand structure in bovine rhodopsin, metarhodopsin-I, and 10-methylrhodopsin from internuclear distance measurements using ^{13}C-labeling and 1-D rotational resonance MAS NMR. *Biochemistry,* **38**, 11316–11324.

37. Buss, V., Kolster, K., Terstegen, F. & Vahrenhorst, R. (1998). Absolute sense of twist of the C12–C13 bond of the retinal chromophore in rhodopsin—semiempirical and nonempirical calculations of chiroptical data. *Angew. Chem. Int. Ed.* **37**, 1893–1895.

38. Fujimoto, Y., Fishkin, N., Pescitellli, G., Decatur, J.,

Berova, N. & Nakanishi, K. (2002). Solution and biologically relevant conformations of enantiomeric 11-*cis*-locked cyclopropyl retinal. *J. Am. Chem. Soc.* **124**, 7294–7302.

39. Buss, V., Sugihara, M., Entel, P. & Hafner, J. (2003). Thr94 and wat2b effect protonation of the retinal chromophore in rhodopsin. *Angew. Chem. Int. Ed.* **42**, 3245–3247.

40. Sugihara, M., Buss, V., Entel, P. & Hafner, J. (2004). The nature of the complex counterion of the chromophore in rhodopsin. *J. Phys. Chem. sect. B,* **108**, 3673–3680.

41. Crozier, P. S., Stevens, M. J., Forrest, L. R. & Woolf, T. B. (2003). Molecular dynamics simulation of dark-adapted rhodopsin in an explicit membrane bilayer: coupling between local retinal and larger scale conformational change. *J. Mol. Biol.* **333**, 493–514.

42. Yan, E. C. Y., Kazmi, M. A., Ganim, Z., Hou, J. M., Pan, D. H. Chang, B. S. W. *et al.* (2003). Retinal counterion switch in the photoactivation of the G protein-coupled receptor rhodopsin. *Proc. Natl Acad. Sci. USA,* **100**, 9262–9267.

43. Birge, R. R. & Knox, B. E. (2003). Perspectives on the counterion switch-induced photoacrivation of the G protein-coupled receptor rhodopsin. *Proc. Natl Acad. Sci. USA,* **100**, 9105–9107.

44. Kusnetzow, A. K., Dukkipati, A., Babu, K. R., Ramos, L., Knox, B. E. & Birge, R. R. (2004). Vertebrate ultraviolet visual pigments: protonation of the retinylidene Schiff base and a counterion switch during photoactivation. *Proc. Natl Acad. Sci. USA,* **101**, 941–946.

45. McRee, D. (1999). XtalView /Xfit—a versatile program for manipulating atomic coordinates and electron density. *J. Struct. Biol.* **125**, 156–165.

46. Fahmy, K., Jäger, F., Beck, M., Zvyaga, T. A., Sakmar, T. P. & Siebert, F. (1993). Protonation states of membrane-embedded carboxylic acid groups in rhodopsin and metarhodopsin II: a Fourier-transform infrared spectroscopy study of site-directed mutants. *Proc. Natl Acad. Sci. USA,* **90**, 10206–10210.

47. Yan, E. C. Y., Kazmi, M. A., De, S., Chang, B. S. W., Seibert, C. Marin, E. P. *et al.* (2002). Function of extracellular loop 2 in rhodopsin: glutamic acid 181 modulates stability and absorption wavelengh of metarhodopsin II. *Biochemistry,* **41**, 3620–3627.

48. Birge, R. R., Murray, L. R., Pierce, B., Akita, M., Balogh-Nair, V. & Nakanishi, K. (1985). Two-photon spectroscopy of locked-11-*cis*-rhodopsin: evidence for a protonated Schiff base in a neutral protein binding site. *Proc. Natl Acad. Soc. USA,* **82**, 4117–4121.

49. Kraulis, P. J. (1991). MOLSCRIPT: a program to produce both detailed and schematic plots of protein structures. *J. Appl. Crystallog.* **26**, 282–291.

50. Merritt, E. A. & Murphy, M. E. P. (1994). Raster3D version 2.0: a program for photorealistic molecular graphics. *Acta Crystallog. sect. D,* **50**, 869–873.

Edited by R. Huber